Journal of Applied Electrochemistry (2005) 35:305–310
DOI 10.1007/s10800-004-7274-5

Calculation of the current density distribution of submicron copper electroplating based on uneven adsorption of poly(ethylene glycol)

BANG-HAO WU, CHI-CHAO WAN* and YUNG-YUN WANG
Department of Chemical Engineering, Tsing-hua University, Hsin-Chu, Taiwan 300
*(*author for correspondence, fax: +886-3-5715408; e-mail: ccwan@mx.nthu.edu.tw)*

Received 12 July 2004; accepted in revised form 23 November 2004

Key words: adsorption, current distribution, model, polyethylene glycol, void-free

Abstract

Uneven adsorption of polyethylene glycol (PEG) along a submicron feature enabling the occurrence of void-free deposition has been identified and we have developed a simplified 1-D model to explain the phenomenon based on the distribution of hydrodynamic driving force along the trench depth. We also verified this new model based on the uneven PEG adsorption via an electrochemical quartz crystal microbalance study. The model shows that with only moderate PEG concentration, void-free deposition can be realized. Some parameters used in the modeling were developed from chronopotentiometry and rotating disc electrode experiments.

1. Introduction

A prime requirement for copper electroplating of IC interconnect is void-free deposition. Development of a process means the establishment of an operational window for parameters, including the composition of the bath, the fluid flow conditions and the applied voltage or current. To reduce the required experimental work, numerical modeling can identify optimal operational conditions from limited experimental data. Several papers have shown simulation results with acceptable accuracy as compared to experimental observations [1–8].

The diffusion–adsorption mechanism is extensively adopted in these models to explain void-free phenomena. However, in cases without leveler, such as JGB, a void-free deposition profile with bump formation on the feature contradicts the predictions by the mechanism. Moffat et al. [3] and West et al. [9] proposed a new mechanism called curvature enhanced accelerator coverage (CEAC) that permits quantitative description of bump emergence. Although these two mechanisms are useful in the interpretation of most published results, they cannot satisfactorily describe a void-free deposition with Polyethylene glycol (PEG) as single additive mentioned in our findings [10], as well as in other papers [11, 12], because without the presence of accelerator, the CEAC mechanism is not applicable. Furthermore, the negligible amount of PEG molecule incorporated within deposition film, which was also found by Hebert [13], is incompatible with the diffusion–adsorption mechanism. So, in this work, we have developed a new model to predict how the geometrical hindrance results in uneven adsorption distribution inside the feature. For simplicity, we assume the aspect ratio of the feature is high enough so that the system can be reduced to a 1-D problem. Some electrochemical experiments were also conducted to determine kinetic parameters needed in our model.

2. Modeling and experiments

2.1. *Modeling formulation*

For a high aspect ratio trench as illustrated in Figure 1, the concentration variation of cupric ion mainly occurs along the y-direction. The validity of a 1-D approach was proven by West et al. [1]. However, as the deposition proceeds, the change of surface geometry due to deposit growth requires the use of the moving boundary algorithm, [14, 15]. The change of trench profile during deposition must eventually conflict with the 1-D (high aspect ratio) assumption and a 2-D model would have to be adopted for overall deposition profile prediction [2–8]. Nevertheless, the major goal of this work is to qualitatively describe how the uneven PEG adsorption on the surface occurs, rather than quantitatively describe the changing deposition profile, so the 2-D model with the moving boundary effect is not necessary.

Material balance along y-coordinate and assuming steady state condition leads to the 1-D governing equation as follows,

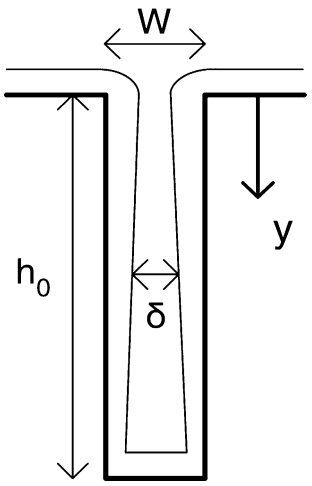

Fig. 1. The schematic diagram of the characteristic lengths used in feature scale simulation.

$$D\frac{\mathrm{d}}{\mathrm{d}y}\left(\frac{\mathrm{d}c}{\mathrm{d}y}\delta(y)\right)+\frac{i}{nF}=0. \tag{1}$$

The corresponding boundary conditions are

$$\begin{cases} at\ y=0, & c=c_{\mathrm{b}} \\ at\ y=h_0, & D\frac{\mathrm{d}c}{\mathrm{d}y}=\frac{i}{nF}, \end{cases} \tag{2}$$

where c_{b} is the bulk concentration of the copper ion. Because the potential variation is limited within each trench, the deposition kinetics can be regarded as first order accompanied with the PEG blocking effect, as shown in Equation 3.

$$\frac{i}{i_{\mathrm{T}}}=i^{*}=\frac{c(1-\theta_{\mathrm{eff}})}{c_{\mathrm{b}}(1-\theta_{\mathrm{T,eff}})}, \tag{3}$$

where i_{T} and $\theta_{\mathrm{T,eff}}$ are the current density and effective surface coverage of PEG at the trench opening, respectively. The maximum effective surface coverage is relevant to the applied current density. For galvanostatic operation at 10 mA cm^{-2}, the maximum effective surface coverage ($\theta_{\mathrm{eff,max}}$) experimentally obtained is around 0.93. If we define the surface coverage of PEG, θ, to be the ratio of the adsorbed PEG molecules to its maximum value, $\dfrac{\Gamma}{\Gamma_{\max}}$, the relation between θ and θ_{eff} can then be formulated as Equation 5.

$$\theta=\frac{\Gamma}{\Gamma_{\max}} \tag{4}$$

$$\theta=\frac{\theta_{\mathrm{eff}}}{\theta_{\mathrm{eff,max}}} \tag{5}$$

According to our previous work [10], the adsorption isotherm of PEG matches the Toth isotherm. Since the Toth parameters are close to 1, we simplify it to a Langmuir type as follows,

$$\frac{\theta}{1-\theta}=K(Re)c_{\mathrm{PEG}}, \tag{6}$$

where $K(Re)$ indicates the adsorption constant could be affected by the Reynolds number. Because the potential gradient is neglected and the PEG incorporation amount is infinitesimal, the only possible reason for uneven adsorption is the variation of adsorption constant in different fluid flow conditions. It has been shown by Kislenko et al. [16] that the adsorption kinetics of poly(ethylene oxide) with molecular weight from 7.1×10^{3} to 847×10^{3} is related to the Reynolds number and the physical properties of adsorbent, for example, the degree of polymerization. Although, in our case, the adsorbent and the adsorbate are different, we could still adopt their idea and assume the adsorption constant is affected by the electrolyte hydrodynamics

$$K=pRe^{q} \tag{7}$$

and Re is equal to $\frac{wR^2}{\upsilon}$, where w is the rotation rate (s^{-1}), R is the RDE radius (cm) and υ is the kinematic viscosity ($\mathrm{cm}^2\ \mathrm{s}^{-1}$). Parameters p and q were then evaluated from experimental results.

The flow inside submicron trenches is much slower than that outside. Takahashi and Gross [17] theoretically showed that the Peclet number within the feature was much smaller than unity, indicating that the transfer of cupric ion was diffusion controlled. Their results show that an eddy circulates inside the trench with velocity about two orders of magnitude lower than the velocity of flow parallel to the wafer just outside the trench [17]. In addition, the fluid shows very low velocity in the region below the primary eddy.

According to Takahashi's work we assume an exponential decay of Reynolds number inside the trench as follows,

$$Re=Re_{\mathrm{T}}e^{(-ya)}, \tag{8}$$

where Re_{T} is the Reynolds number at the top of the trench. According to Takahashi's work, the eddy diameter is equal to the width of the trench and Re at $y=W$ is less than Re_{T} by two orders of magnitude. For a 0.4-cm diameter RDE with a rotation speed of 100 rpm and a kinematic viscosity of 0.0397 $\mathrm{cm}^2\ \mathrm{s}^{-1}$, the value of Re_{T} and parameter a in Equation 8 will be 10.55 and 184206.8 cm^{-1}, respectively.

The applied current density (i_p) at 10 mA cm^{-2} is the average of all the local current densities and thus the relation between i_{T} and i_{p} is governed by Equation 9.

$$i_{\mathrm{p}}=\frac{\iint i\mathrm{d}A}{\iint \mathrm{d}A}=\frac{i_{\mathrm{T}}\int_0^{h_0}c(1-\theta_{\mathrm{eff}})\mathrm{d}y}{h_0c_{\mathrm{b}}(1-\theta_{\mathrm{T,eff}})}\Rightarrow i_{\mathrm{T}}=\frac{i_{\mathrm{P}}}{\int_0^1 i^{*}\mathrm{d}y^{*}} \tag{9}$$

The governing equations, boundary conditions as well as the electrode kinetic equations were then converted

into dimensionless form and are listed in Table 1 with all the dimensionless terms defined as follows,

$$\delta^* = \frac{\delta}{h_0}, y^* = \frac{y}{h_0}, c^* = \frac{c}{c_b}, i^* = \frac{i}{i_T} \quad (10)$$

A finite difference method was then applied to solve the current distribution. Iteration of i^* stops when the difference between the guessing values and the calculated results is smaller than the set tolerance.

2.2. *Experimental*

For the determination of adsorption parameters shown in Equation 7, the adsorption isotherm was evaluated at three different RDE rotation speeds, i.e. 100 rpm, 10 rpm and 1 rpm. The corresponding Reynolds numbers were 10.55, 1.055 and 0.1055, respectively. These three rotation speeds were chosen because the data obtained from a flat surface could then correspond to the various positions inside the trench based on Equation 8. For instance, at 100 rpm the fluid velocity is equal to the velocity at the trench opening predicted by Takahashi and Gross [17]. The adsorption isotherm was evaluated based on chronopotentiometry result by comparing steady-state applied voltages with or without PEG. The electrolyte composition was 0.2 M $CuSO_4$, 1 M H_2SO_4 and 180 ppm Cl^- with PEG (molecular weight $\sim$ 3200) in various concentrations from 10^{-8} M to 10^{-5} M. A Platinum RDE (0.4 cm in diameter) was first deposited with copper at 1 mA for 180 s in a pre-deposition bath. The electrode was then transferred into the test bath and, after immersion for 30 s, the chronopotentiometry experiment was started. Although the system may not fully reach steady-state adsorption in a short period with low PEG concentration as previously observed [10], we assume that 180-s deposition period is long enough for simulation. Actually we found a very good linear relation between ln K and ln Re (Figure 4), which also implies the approximation of steady-state at 180 s is justified. A stripping bath was used to strip off copper at 0.2 V with respect to open circuit potential (OCP) for 120 s and then the residual copper was chemically removed with piranha agent (H_2O_2:H_2SO_4=1:3 in volume) in order to obtain fresh surface conditions on the platinum electrode.

An electrochemical quartz crystal microbalance (EQCM) was used to verify whether the amount of incorporated PEG is negligible. A gold microbalance electrode was first deposited with copper at 1 mA for 30 s. The electrode was then transferred into a stagnant analyzing bath for cyclic voltammetric tests at 10 mV s^{-1} sweep rate and potential between − 0.2 V and 0.1 V with respect to OCP. The composition of the analyzing bath was 10^{-6} M PEG addition into the same base electrolyte as the chronopotentiometry experiment.

The cell was connected to an Autolab (ECO Chemie, Holland) potentiostat coupled to an EG&G QCA917. All chemicals used were of analytical grade.

Table 1. Dimensionless equations used in the model. The definition of ξ is $\frac{i_T h_0}{nDFc_b}$

Governing equation	$\frac{d\delta^*}{dy^*}\frac{dc^*}{dy^*} + \delta^*\frac{d^2c^*}{dy^{*}2} + i^*\xi = 0$
Boundary conditions	at $y^* = 1$, $\frac{dc^*}{dy^*} = i^*\xi$
	at $y^* = 0$, $c^* = 1$
Electrode kinetics	$i^* = c^*\frac{(1-\theta_{eff})}{(1-\theta_{T,eff})}$

3. Results and discussions

Figure 2(a) and (b) show the CV results for electrolytes without and with PEG, respectively. The corresponding frequency data of EQCM are also included. As shown in Figure 2(a), the frequency decreased with respect to the deposition current and increased as the stripping started. The results are reasonable since the deposition of copper increases the mass on the quartz and thus reduces its frequency. The rate of the frequency changes also agrees with the change in current.

However, in the case of PEG added to the bath, as shown in Figure 2(b), an different frequency response occurred. Although the current potential response was similar to Figure 2(a), the frequency change on the quartz was clearly different. The frequency initially increased until the potential scan was reversed from the vertex potential at −0.6 V vs SSE. In the stripping period, the frequency still decreased initially, even with a faster rate compared to the backward scan of the deposition period near OCP (−0.4 V). Because the negative current in the deposition period implies that cupric ions are reduced, the only possible reason for the increase in frequency is desorption of the originally adsorbed PEG. If mass loss because by PEG desorption is larger than the mass addition by deposition, the net mass change would be negative. If the increase in deposition current results from the increase in free active sites on the electrode surface where the originally adsorbed PEG molecules are incorporated into the deposit film, the change in frequency should decrease rather than increase. So the EQCM results imply that, the PEG molecules immediately desorb from the electrode surface as deposition proceeds.

The mechanism of PEG desorption is related to the change in electrode surface charge. According to Frumkin's work, the maximum adsorption occurs at the potential of zero charge (pzc) of the electrode [18]. Larger deviation from the pzc means fewer PEG molecules being able to adsorb on the electrode surface. So, in the reverse scan of the deposition current, the deviation from pzc diminishes, so that PEG molecules adsorb back to the electrode surface along with copper deposition and the frequency of the EQCM consequently decreases.

To obtain the adsorption kinetic parameters shown in Equation 7, we then did chronopotentiometric experiments with different RDE rotation speeds. Figures 3(a)–(c) show the adsorption isotherms of PEG at 100 rpm,

10 rpm and 1 rpm, respectively. The calculation of surface coverage is based on the formulation derived in our previous work [10] and two of the three cases (100 rpm, 10 rpm) show good agreement with the Langmuir isotherm, where the R^2 values are all larger than 0.96. More significant deviation appears in the 1 rpm case, which may be owing to the instrument sensitivity, since 1 rpm is the lowest controllable RDE rotation speed in our equipment.

A comparison among the values of the adsorption constants shows that the larger the hydrodynamic driving force, the larger is the adsorption constant. The result demonstrates that the RDE rotation speed affects PEG adsorption behavior. The linearity of ln *Re* and ln *K* can be found in Figure 4, with *q* and *p* being 0.2456 and 1.196×10^7, respectively. The R^2 closely approaches unity, indicating that the use of Kislenko's model is valid. This result indicates that the adsorption of PEG on copper in different hydrodynamic conditions follows the behavior proposed by Kislenko et al. [16].

Substituting the obtained adsorption parameters into our model, the effective surface coverage distribution along the y-coordinate was obtained, as shown in Figure 5. With 10^{-7} M PEG, the highest θ_{eff} is only around 0.55 and the amount of PEG adsorbed at the bottom of the trench is approximately zero. In cases of high PEG concentration, i.e. 10^{-5} M and 10^{-4} M, although the effective surface coverage at the bottom is high enough, the variation of θ_{eff} along the y direction is not sufficient because the concentration of PEG is

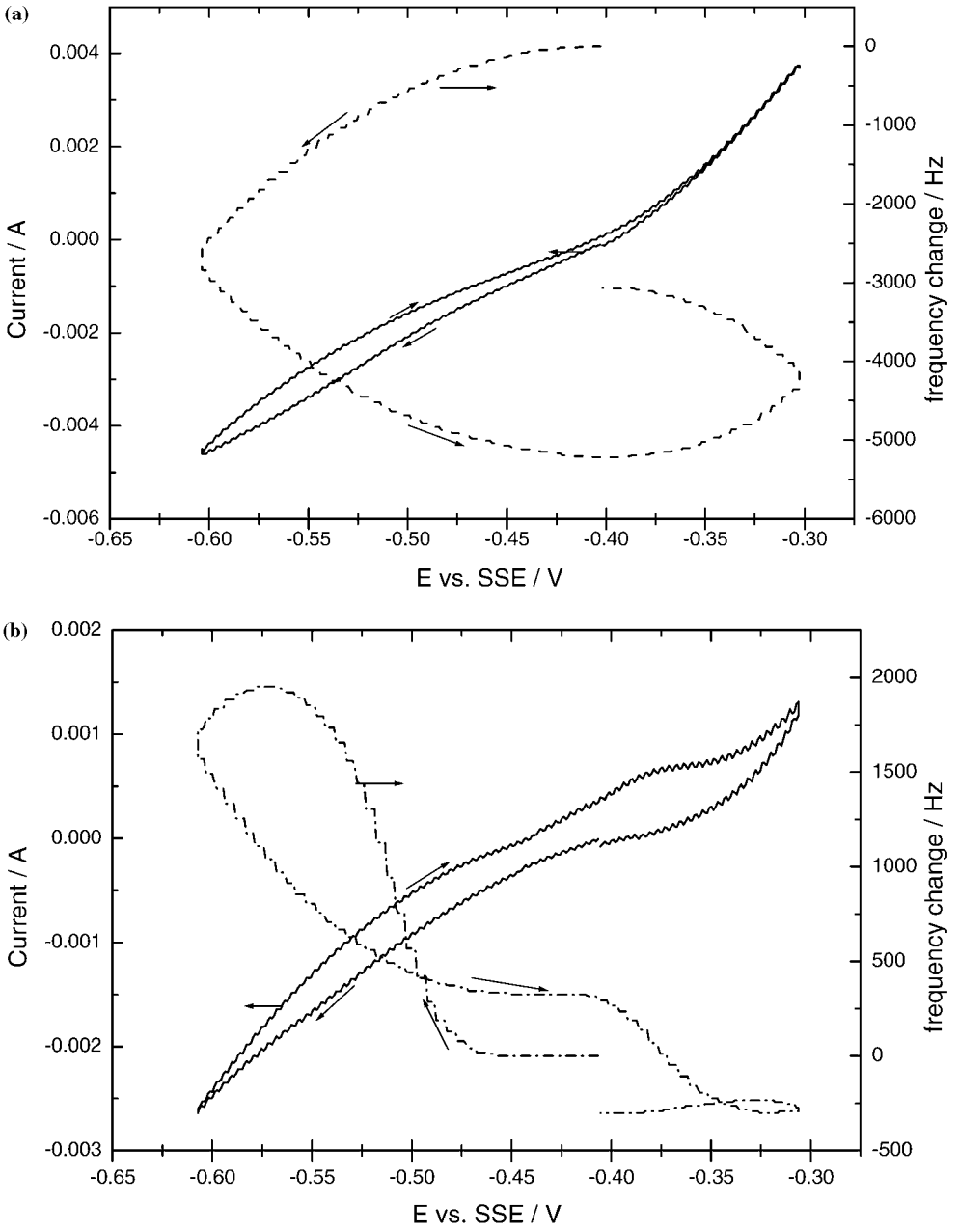

Fig. 2. (a) Top and (b) Down. CV and its corresponding EQCM frequency change. Frequency change is extremely different between cases without (a) and with (b) 10^{-6} M PEG.

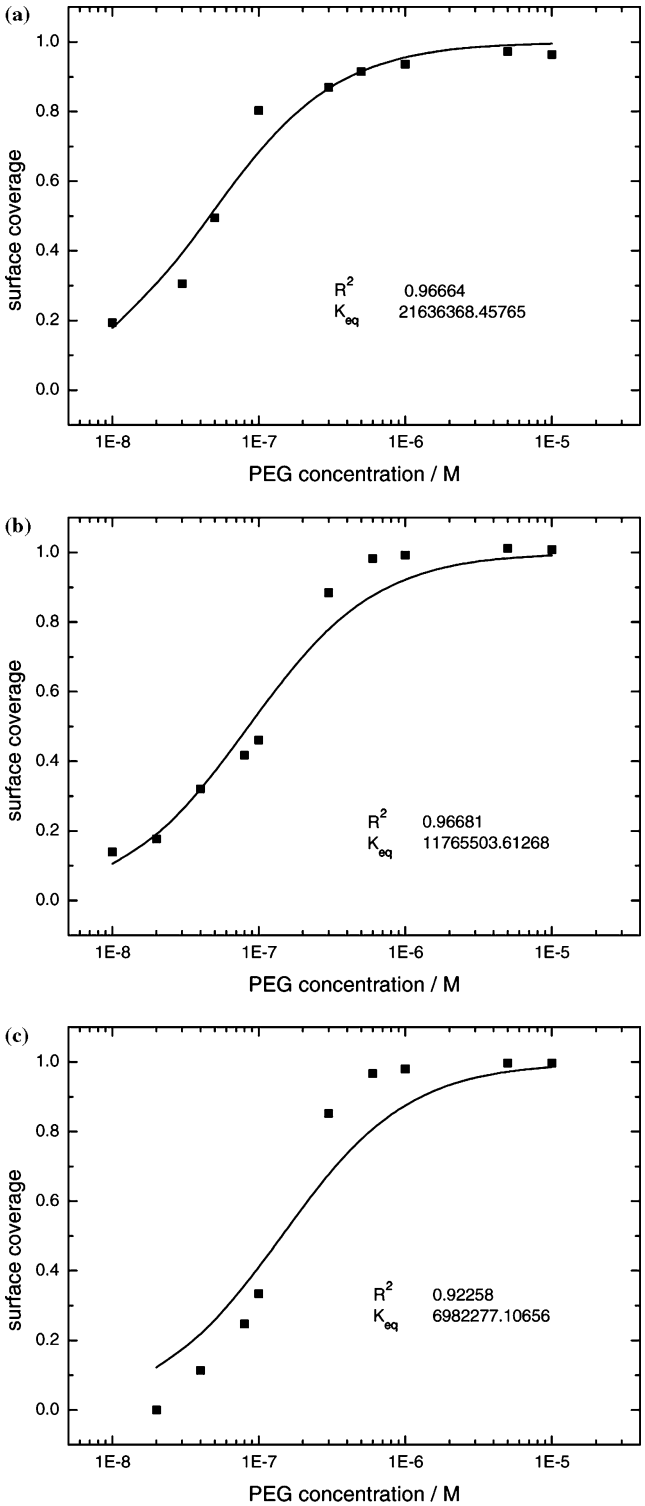

Fig. 3. (a)–(c). Adsorption isotherm of PEG in different RDE rotation speeds. Rotation speeds in (a), (b) and (c) are 100 rpm, 10 rpm and 1 rpm, respectively. Langmuir isotherm is found with acceptable agreement with experimental data.

extremely high and limits the variation of θ_{eff} due to hydrodynamics. Only in moderate concentrations of PEG, (10^{-6} M) is the difference between external θ_{eff} and the bottom θ_{eff} the largest. This simulation result is consistent with the interpretations presented in our previous work [10].

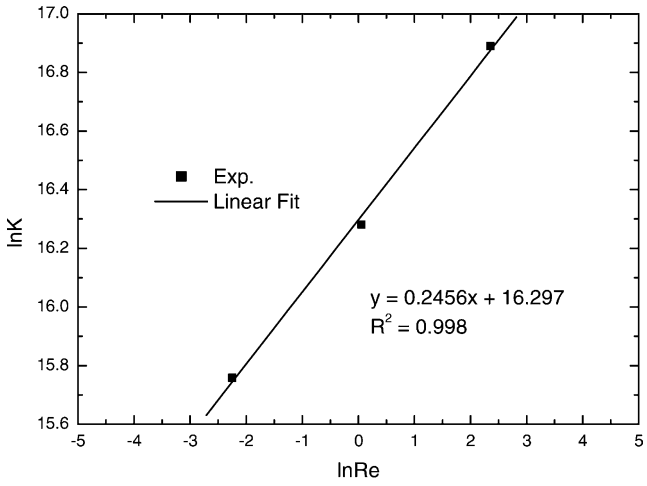

Fig. 4. Fitting for the adsorption kinetic parameters shown in Equation 7.

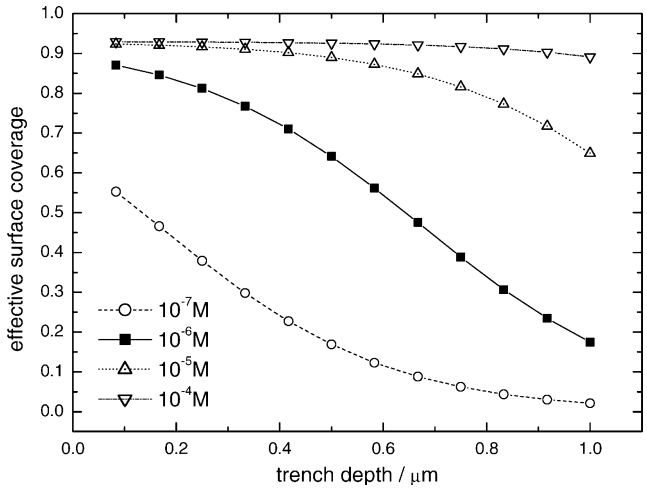

Fig. 5. Distribution of θ_{eff} with respect to the trench depth. Significant uneven adsorption of PEG is found in moderate PEG concentration, i.e. 10^{-6} M.

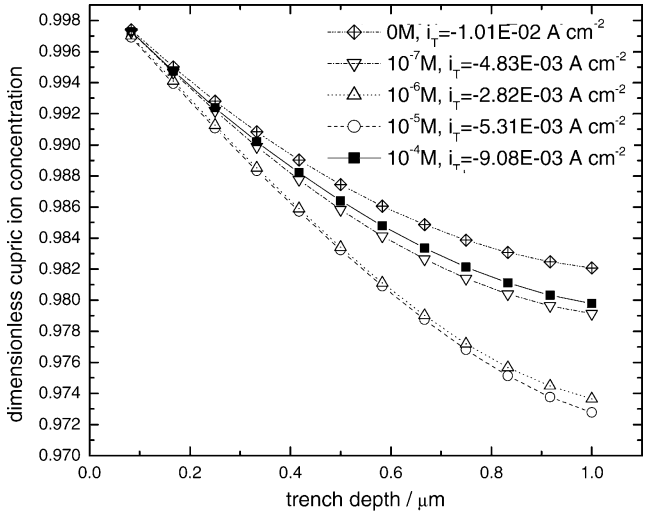

Fig. 6. The distribution of dimensionless cupric ion concentration within the trench depth under various PEG concentrations.

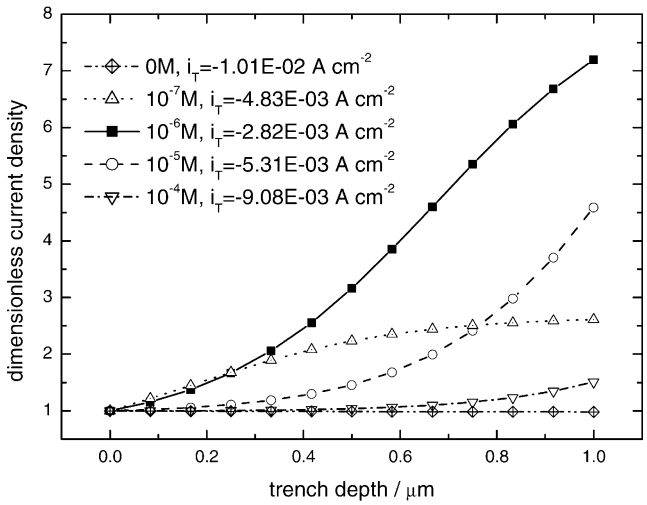

Fig. 7. The dimensionless current density with respect to the trench depth under various PEG concentrations.

The distribution of dimensionless cupric ion concentration within the trench is shown in Figure 6. The cupric ion concentration decreases as the trench depth increases because of cupric ion consumption. The deviations in cupric ion concentration at the trench bottom from that at the trench opening in 10^{-5} M and 10^{-6} M PEG cases are relatively larger, which may be attributed to the significant θ_{eff} variation of PEG in these two cases.

Dimensionless current density distribution along the trench depth by simulation is shown in Figure 7. For electrolyte without PEG, the current density at the bottom is smaller than at the top because of the concentration gradient of cupric ions. The presence of PEG reverses the tendency of i^* distribution and results in higher bottom current density. The largest bottom i^*, approaching 8, occurs in the 10^{-6} M PEG case. In the low (10^{-7} M) and high concentration (10^{-5} M and 10^{-4} M) cases, because the effective surface coverage is either inadequately or oversaturatedly distributed, the bottom i^* is less than that in the 10^{-6} M case. Although our simulation cannot describe the final current distribution since the moving boundary effect was not included, the simulation results still provide solid support to our previous finding [10], in which we proposed a single additive system with PEG could lead to void-free deposition by an uneven adsorption mechanism. The close agreement between the modeling prediction and the experimental data also indicates the validity of our choosing Equation 8 for the velocity distribution in the model. However, the agreement is also realized because our system and Takahashi's system are based on the same trench width (i.e. 0.25 μm). Additional work is required on calculating velocity profile within the trench if one wants to apply our model for other trench dimensions, rather than directly use the approximation of Equation 8.

4. Conclusions

The uneven adsorption of PEG along a submicron feature enables void-free deposition using a single additive. A one-dimensional model was developed which shows that the hydrodynamic driving force varies along the trench depth and results in uneven PEG adsorption. The ratio of the bottom current density to the top current density is relatively high at a moderate PEG concentration (10^{-6} M) as compared to the insufficient (10^{-7} M) or oversaturated ($> 10^{-5}$ M) PEG cases. The frequency data obtained with EQCM in CV experiments demonstrates the incorporation rate of PEG into deposit film is negligible.

Acknowledgement

This work was supported by the National Science Council (Project 90-2214-E007-007) and Chang Chun Petrochemical Corporation in Taiwan.

References

1. A.C. West, C.C. Cheng and B.C. Baker, *J. Electrochem. Soc.* **145** (1998) 3070.
2. T.J. Pricer, M.J. Kushner and R.C. Alkire, *J. Eelectrochem. Soc.* **149** (2002) C406.
3. T.P. Moffat, D.Wheeler, W.H. Huber and D.Josell, *Electrochem. Solid-State Lett.* **4** (2001) C26.
4. D.Varadarajan, C.Y. Lee, A.Krishnamoorthy, D.J. Dquette and W.N. Gill, *J. Eelectrochem. Soc.* **147** (2000) 3382.
5. T.P. Moffat, D.Wheeler, W.H. Huber and D.Josell, *Electrochem. Solid-State Lett.* **5**(4) (2002) C49.
6. M.Georgiadou and D.Veyret, *J. Eelectrochem. Soc.* **149** (2002) C324.
7. R.Chalupa, Y.Cao and A.C. West, *J.Appl. Electrochem.* **32** (2002) 135.
8. Y.Cao, P.Taephaisitphongse and A.C. West, *J.Electrochem. Soc.* **148** (2001) C466.
9. A.C. West, S.Mayer and J.Reid, *Electrochem. Solid-State Lett.* **4**(7) (2001) C50.
10. B.H. Wu, C.C. Wan and Y.Y. Wang, *J.Appl. Electrochem.* **33** (2003) 823.
11. S.C. Chang, J.M. Shieh, K.C. Lin, B.T. Dai, T.C. Wang, C.F. Chen, M.S. Feng, Y.H. Li and C.P. Lu, *J. Vac. Sci. Technol. B*, **B20** (2002) 1311.
12. M.Hayase, M.Taketani, K.Aizawa, T.Hatsuzawa and K.Hayabusa, *Electrochem. Solid-State Lett.* **5** (2002) C98.
13. K.R. Hebert, *J.Electrochem. Soc.* **148** (2001) C726.
14. J.O. Dukovic and C.W. Tobias, *J.Electrochem. Soc.* **137** (1990) 3748.
15. P.C. Andricacos, C.Uzoh, J.O. Dukovic, J.Horkans and H.Deligianni, *IBM J.Res. Dev.* **42** (1998) 567.
16. V.N. Kislenko, AD.A. Berlin and M.A. Moldovanov, *J. Colloid Inter. Sci.* **173** (1995) 128.
17. K.M. Takahashi and M.E. Gross, *J.Electrochem. Soc.* **146** (1999) 4499.
18. E.Gileadi, 'Electrode Kinetics for Chemists, Chemical Engineers and Materials Scientists', (VCH Publishers, New York, 1993).